

EFFECT OF LARGE-SCALE INHOMOGENEITY OF SOLAR WIND VELOCITY ON DISTRIBUTION OF DIRECTIONS OF INTERPLANETARY MAGNETIC FIELD VECTOR

D.V. Erofeev

*Ussuriisk Astrophysical Observatory, FEB RAS,
Ussuriisk, Russia, dve_08@mail.ru*

Abstract. Using data with hourly resolution obtained in the near-Earth heliosphere in 1965–2014, we have calculated statistical characteristics of the angles describing the direction of the interplanetary magnetic field (IMF): root-mean-square deviations of azimuth and elevation angles, asymmetries of their distributions, and coefficient of correlation of the angles. It has been shown that the above characteristics vary in the course of solar cycle, and some of them change their signs when the solar polar magnetic field reverses. The results obtained from the experimental data analysis are compared with a model describing transport of large-scale disturbances of IMF lines by the inhomogeneous solar

wind. The comparison shows that the variations in the IMF angular distribution in the course of solar cycle probably occur due to the appearance of the large-scale latitudinal gradient of solar wind velocity during solar minima. In addition, the IMF angular distribution has been found out to be substantially affected by the longitudinal velocity gradient in trailing parts of high-speed streams and short-term local-scale variations in velocity gradients.

Keywords: interplanetary magnetic field, solar wind, solar cycle.

INTRODUCTION

The interplanetary magnetic field (IMF) experiences significant deviations from the mean direction, which approximately corresponds to the well-known Parker spiral [Kovalenko, 1983; Forsyth et al., 1996; Burlaga, Ness, 1997; Veselovsky, Tarsina, 2001; Borovsky, 2010; Xu et al., 2015]. Such deviations are partially caused by the presence of strong solar wind (SW) inhomogeneities such as interaction regions of fast and slow streams and disturbances generated by solar activity [Schwadron, McComas, 2005; Borovsky, 2010]. However, in relatively undisturbed SW regions the IMF modulus and vector direction also exhibit random fluctuations. The two-dimensional statistical distribution of angles characterizing the IMF direction will be called the IMF angular distribution. The angles specifying the IMF vector direction are usually measured from the line connecting the center of the Sun with an observation point. One of these angles is measured in the east-west direction (azimuth); and another, in the north-south direction (elevation). They are sometimes referred to as longitude and latitude. Characteristics of the IMF angular distribution depend on the length of measurement averaging interval [Veselovsky, Tarsina, 2001; Borovsky, 2010], which is most likely due to the wide spectrum of temporal and spatial scales of IMF direction fluctuations. In this paper, we are interested in large-scale variations of IMF so we examine the IMF angular distribution, using hourly averaging data.

In the experimental data analysis, statistical characteristics of IMF azimuth and elevation are generally considered separately. The behavior of root-mean-square deviations (RMSD) of angles in the ecliptic plane has been studied in considerable detail; in particular it has been shown that they increase with heliocentric distance [Borovsky, 2010]. As deduced from the

hourly average measurements made in near-Earth orbits from 1963 to 2008, azimuth and elevation RMSDs undergo small time variations, which do not show a pronounced relationship with solar cycle phase [Borovsky, 2010]. However, Burlaga, Ness [1997] have previously determined that RMSD of elevations slightly increases during high solar activity.

Several studies have considered the shape of statistical distributions of IMF azimuths and elevations. In the low-latitude region of the heliosphere, the distribution of IMF azimuths, on average, does not show a significant asymmetry (speaking of the azimuth distribution asymmetry, we mean the asymmetrical shape of two peaks of bimodal distribution rather than the height difference between these peaks). A variation was observed in elevation and azimuth distributions during the solar cycle [Burlaga, Ness, 1997; Borovsky, 2010] and a difference was noted between these distributions in slow SW and high-speed streams [Borovsky, 2010]. The above papers did not, however, consider any quantitative measure characterizing the shape of the distributions. Erofeev [2014] has quantitatively studied the asymmetry in the distribution of IMF elevations, using measurements in the near-Earth region of the heliosphere over four solar cycles. The distribution of IMF elevations during solar minima was revealed to be slightly asymmetric with the skewness sign dependent on the orientation of the solar polar magnetic field but independent of the IMF sector polarity. Furthermore, the analysis of measurements obtained in the ecliptic plane has shown that during solar minima the IMF angular distribution becomes substantially two-dimensional: fluctuations of IMF azimuth and elevation significantly correlate, with the sign of the correlation coefficient depending on the orientation of the solar

polar magnetic field [Lyatsky et al., 2003; Erofeev, 2014]. Measurements made by the Ulysses spacecraft allowed us to compare IMF angular distributions at low and high heliographic latitudes. From the analysis of Helios 1, Helios 2, and Ulysses data Erofeev [2014] have deduced that during low solar activity the IMF azimuth and elevation correlate in the low-latitude region at heliocentric distances from 0.3 to 5 AU, and did not correlate in polar zones of the heliosphere. It has also been found out that in polar zones during periods close to solar minima the IMF azimuth distribution is strongly asymmetric in contrast to that in the low-latitude region [Forsyth et al., 1996].

It follows from the above that the IMF angular distribution depends on solar cycle, during low solar activity its characteristics in the low-latitude and polar zones differ substantially. The variations in the IMF angular distribution characteristics occurring in a solar cycle in the low-latitude heliosphere may be associated with the varying degree of SW inhomogeneity. In particular, the IMF angular distribution may be affected by the stable latitudinal gradient of SW velocity, which is observed in the equatorial zone of the heliosphere during solar minima [McComas et al., 2000]. Polar SW during minima of the 11-year solar cycle is relatively homogeneous, whereas in the low-latitude zone there are stream interaction regions and large-scale SW velocity gradients. Thus, the differences between the characteristics of the IMF angular distribution at low and high heliolatitudes are probably also due to the distinction in degree of SW stream inhomogeneity.

As noted above, the IMF angular distribution characteristics depend on the measurement averaging interval length. This is due to the fact that magnetic field fluctuations have a wide spectrum of spatial and temporal scales. The low-frequency part of the spectrum contains large-scale relic magnetic field structures, which are formed in near-Sun space and remain more or less unchanged up to heliocentric distances of several astronomic units. The high-frequency part of the spectrum of IMF fluctuations is formed due to the development of turbulence when the relic structures decay with distance from the Sun [Bruno, Carbone, 2005]. When selecting a particular length of the data averaging interval, the contribution of turbulence is suppressed and the IMF angular distribution characterizes properties of the relic magnetic field structures. According to Tu, Marsch [1993], such structures can be regarded as transverse perturbations of magnetic field lines. These perturbations can be formed by motions of magnetic footpoints caused by plasma motions in the photosphere or by magnetic reconnection processes in the solar corona [Giacalone, 2001; Giacalone, Jokipii, 2004; Ulrich, Tran, 2016].

The relic nature of the large-scale perturbations of IMF lines does not imply that they do not experience changes when transported from near-Sun space to the point where IMF is measured. Even in the framework of the kinematic approach, i.e. assuming that magnetic field line perturbations are passively transported by the SW stream, the shape of these perturbations changes due to the twisting of IMF into the Parker spiral and the impact of SW velocity gradients (see [Kovalenko, 1983]

and references therein). The kinematic approach has been applied by Giacalone [2001], who derived equations describing the transport of the transverse perturbations of IMF lines by the solar wind, which were induced by motions of magnetic footpoints on the Sun. Since the SW velocity is set independent of heliographic coordinates, these equations describe the evolution of perturbations associated with the radial expansion of SW and twisting of IMF into the Parker spiral. Giacalone, Jokipii [2004] have found out that the model correctly describes the variance of IMF direction fluctuations and its dependence on the heliocentric distance. Erofeev [2017] has analyzed a simple kinematic model in terms of the effects of latitudinal and longitudinal gradients of SW velocity on transverse perturbations of IMF lines. Calculations made in the said paper have shown that the consideration of the SW stream inhomogeneity allows us to qualitatively explain the behavior of asymmetry in IMF azimuths and elevations as well as the appearance of the correlation between IMF azimuth and elevation during low solar activity periods.

The purpose of this work is to qualitatively and quantitatively study the influence of kinematic effects, associated with the large-scale SW inhomogeneity, on the IMF angular distribution characteristics. The first stage of the solution of this problem involves obtaining quantitative characteristics describing the IMF angular distribution variation during the solar cycle from experimental data. To do this, we process magnetic field measurements made in the near-Earth region of the heliosphere over four solar cycles. The measurement processing method is described in Section 1, and the experimental data analysis results are presented in Section 2. The second stage of the solution of the problem with the aid of the model equations derived in [Erofeev, 2017] involves calculating the IMF angular distribution characteristics similar to those obtained from the experimental data analysis. The model and methods of selecting parameters characterizing SW properties are described in Section 3. Section 4 qualitatively and quantitatively compares the model calculations with the experimental data processing results. Section 5 presents conclusions and discussions.

1. EXPERIMENTAL DATA AND METHOD OF THEIR ANALYSIS

1.1. Experimental data

As experimental data for our study we have utilized measurements of IMF vector and SW plasma parameters made by a number of satellites in the near-Earth region of the heliosphere in 1965–2014. The measurements are averaged over one hour and are published in the NASA NSSDC database as the well-known catalog OMNI-2. We have used measurements from the reference system RTN: the unit vector \mathbf{e}_R is directed along the line connecting the center of the Sun with an observation point; the unit vector \mathbf{e}_T is parallel to $\mathbf{\Omega} \times \mathbf{e}_R$, where $\mathbf{\Omega}$ is the vector of angular solar rotation rate, $\mathbf{e}_N = \mathbf{e}_R \times \mathbf{e}_T$ (see Figure 1, *a*).

For the analysis we have selected the time intervals during which a spacecraft was outside strongly disturbed

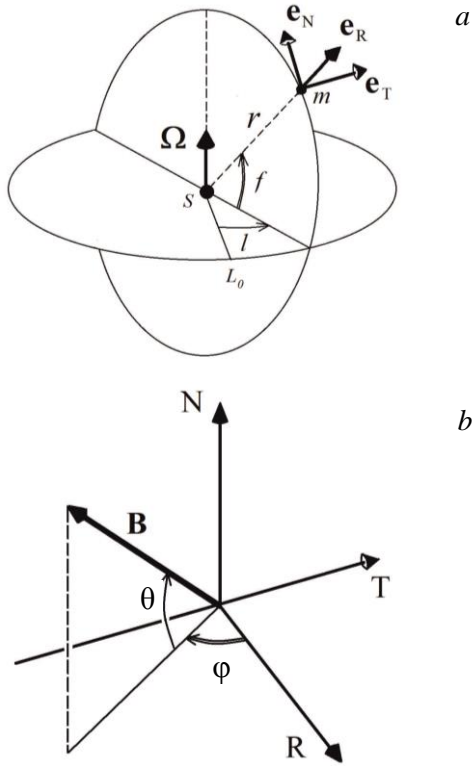


Figure 1. Coordinate systems RTN and (r, f, l) in use. The symbols s and m denote the solar center and the point, where the measurements are made, L_0 is the beginning of longitude reading (other notations are described in the text) (a); explanation of the method for determining the ϕ and θ angles describing the direction of the magnetic field vector \mathbf{B} (b)

SW. By the strong disturbances are meant in particular the interaction region of fast and slow SW streams (including high-speed stream fronts and compressions preceding them) and vicinities of IMF sector boundaries. The strong disturbances are also considered to be sharp increases in the plasma density or magnetic field strength, intervals with unstable orientation of the IMF vector, and other parameter variations, which may morphologically be related to solar eruptive phenomena. The disturbances were excluded from datasets, using software able to identify disturbances visually by observing IMF variations and SW plasma parameters on the screen (no formal numerical criteria were applied in this case). Measurements within each of the intervals selected for the analysis were labeled as belonging to an IMF sector of particular polarity as well as to one of two types of quasi-stationary streams — slow SW or trailing part of high-speed stream. The selected measurements accounted for $\sim 60\%$ of the initial data. The angles ϕ (azimuth) and θ (elevation), which contain all information about the IMF vector direction, were used directly for the analysis:

$$\tan \phi = -\frac{B_T}{B_R}, \quad (1a)$$

$$\tan \theta = \frac{B_N}{\sqrt{B_R^2 + B_T^2}}, \quad (1b)$$

where B_R , B_T , B_N are the IMF vector components in RTN (directions of readings of ϕ and θ are shown in Figure 1, b).

The selection of measurements has yielded two samples, one of which included IMF measurements in slow SW and another, those in trailing parts of high-speed streams. Figure 2, a shows SW velocity distributions for the two samples. These distributions are overlapped within a small interval at ~ 450 km/s because in the regions of slow and fast SW streams the velocity fluctuates considerably. The data selected for the analysis also contains information about belonging to an IMF sector of certain polarity. Figure 2, b displays ϕ azimuth distributions calculated separately for the intervals when measurements were made in positive or negative IMF sectors. Unimodality of these distributions suggests a quite effective separation of measurements according to their belonging to IMF sectors of different polarities.

1.2. Method for analyzing experimental data

When calculating the IMF angular distribution characteristics, we have used a method described by Mardia [1972]. Let there be a sample of values of a one-dimensional random variable characterizing the direction of a vector (to be specific, take the IMF azimuth angle ϕ). The mathematical expectation ϕ_m of ϕ is estimated using the relation

$$\tan \phi_m = \frac{\langle \sin \phi \rangle}{\langle \cos \phi \rangle}. \quad (2)$$

Hereafter, angular brackets denote averaging over the data sample. The variance is estimated using the expression

$$D_\phi = 2(1 - \rho), \quad (3)$$

where $\rho^2 = \langle \sin \phi \rangle^2 + \langle \cos \phi \rangle^2$. In this paper, we examine the behavior of two characteristics of the ϕ distribution: RMSD of azimuth S_ϕ

$$S_\phi = D_\phi^{1/2} \quad (4)$$

and skewness A_ϕ :

$$A_\phi = -\frac{\langle \sin 2(\phi - \phi_m) \rangle}{D_\phi^{3/2}}, \quad (5)$$

as well as the behavior of similar characteristics of IMF elevation distribution, S_θ and A_θ . Estimates (2)–(5) are invariant with respect to the choice of the beginning of reading of ϕ , variance and asymmetry formulas coinciding with ordinary expressions for parameters of distribution, specified on line, in the lowest order of the expansion in powers $\phi - \phi_m$. Obviously, the described method is ill-suited for the analysis of the bimodal distribution such as the distribution of IMF azimuths. This difficulty can be eliminated due to the fact that the data selected for the analysis is separated according to its belonging to IMF sectors of different polarities, hence each of the samples has a unimodal distribution of ϕ angles (see Figure 2, b).

The above method is intended for the study of one-dimensional angular variables and is used to analyze the ϕ and θ distributions. Since properties of these distributions differ significantly (see Section 2), this approach is considered to be valid to a certain extent. The

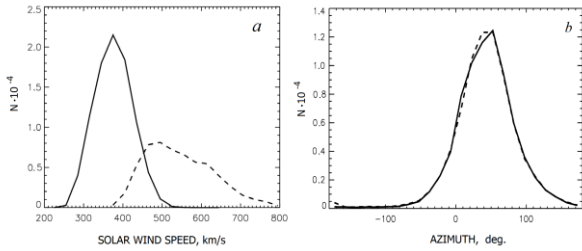


Figure 2. Distribution of data selected for the analysis by solar wind velocities (low-speed wind (solid line); trailing parts of high-speed streams (dashed line)) (a); IMF azimuth distribution for measurements assigned to positive and negative IMF sectors (solid and dashed lines respectively) (b). The distribution for the negative IMF sector is shifted by 180° in azimuth

statistical relationship between fluctuations of φ and θ is, however, left out of consideration. To fill this gap, we examine the angular correlation coefficient, which is calculated by the formula

$$C_{\varphi\theta} = \frac{\langle \sin(\varphi - \varphi_m) \sin(\theta - \theta_m) \rangle}{\sqrt{D_\varphi D_\theta}}. \quad (6)$$

Mardia [1972] did not discuss the method of calculating statistical errors in distribution parameter estimates; therefore we have obtained the estimated errors from numerical experiments, using a random number generator.

2. RESULTS OF THE EXPERIMENTAL DATA ANALYSIS

Parameters of the IMF angular distribution were calculated for an interval of two years, which was sequentially shifted by one year. The great length of the data averaging interval was chosen to provide an acceptable level of statistical errors in estimating the asymmetry of φ and θ distributions. The calculations have shown that the behavior of the IMF angular distribution characteristics is in general the same in IMF sectors of different polarities, except for the difference between mean values of φ by 180° . This allowed us to improve the statistical support of the estimates by combining data for both the IMF sectors after excluding the mean values of φ .

Figure 3 presents estimates of RMSD of φ and θ calculated by Formulas (3), (4) separately for slow SW (Figure 3, a) and trailing parts of high-speed streams (Figure 3, b). It can be seen that RMSDs of azimuths S_φ are systematically greater than those of elevations S_θ — their difference is, on average, 12° . It can also be noted that RMSDs of φ and θ in slow SW are on average greater than those in fast SW (the difference is $\sim 4^\circ$). Since probable errors in determining S_φ and S_θ do not exceed 1° , all the above systematic differences between RMSDs of angles can be considered reliable. In slow SW, S_φ undergoes relatively small (amplitude of $\sim 15\%$ of the mean value) but quite pronounced variations during the 11-year cycle, S_φ maxima occurring during solar minima. In addition to this variation, S_φ exhibits small increases near solar maxima. In fast SW, S_φ has

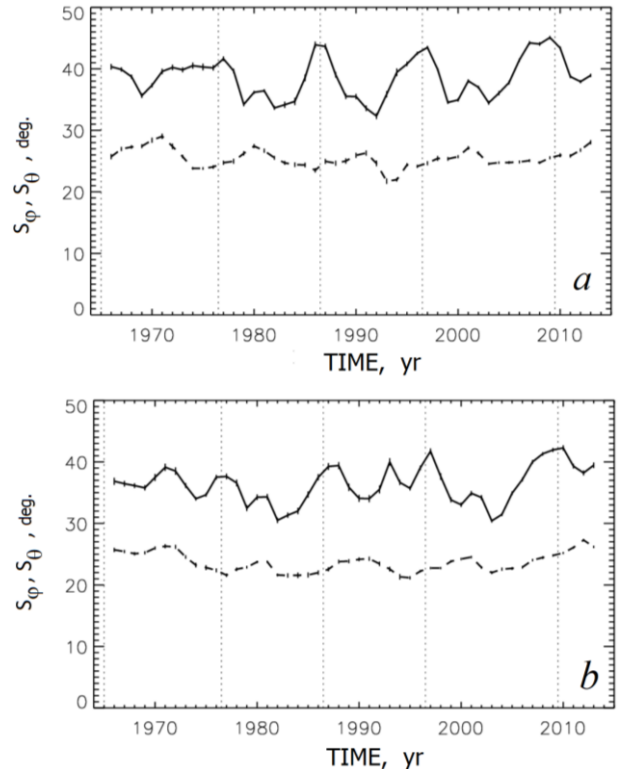


Figure 3. Root-mean-square deviations of IMF azimuths S_φ (solid line) and elevations S_θ (dashed line) as a function of time: slow SW (a); trailing parts of high-speed streams (b). Vertical dashes indicate probable errors of estimates. Solar minima are marked with vertical dotted lines

comparable maxima both in minima of the 11-year cycle and during high solar activity. S_θ shows small increases during high solar activity, S_θ minima not exhibiting a distinct localization in relation to solar minima. The S_θ increases associated with high solar activity have low amplitude (several degrees) but are independently detected from measurements in slow and fast SW, which confirms their reality. It can be concluded that variations in angular RMSDs comprise two components. One of them represents variations occurring in antiphase with solar activity variation and is typical only of S_φ . The second component manifests itself as a small increase in RMSD of both the angles, which occurs near maxima of the 11-year cycles. Besides variations associated with the 11-year cycle, RMSDs of azimuths and elevations feature a long-term nonlinear trend of several degrees, and the characteristic time exceeds the length of the studied time series (this trend is more pronounced in fast SW).

Time dependences of RMSDs of IMF azimuth and elevation (in GSE) have been considered in [Borovsky, 2010], where these parameters were evaluated from OMNI-2 hourly data by approximating the angular distributions by Gaussians. Despite the difference between the estimation methods, the RMSDs of angles we and Borovsky [2010] derived differ, on average, by only a few degrees. The result of our calculation, however, shows more clearly the relationship of variations in RMSD of φ and θ with solar cycle. Burlaga, Ness [1997] have estimated RMSD of IMF elevation distribu-

tion from OMNI-2 hourly average measurements by approximating the distribution by Gaussian. These authors have found out that RMSD of elevations increases by $\sim 5\%$ during high solar activity, which is consistent with the results of our calculations.

Figure 4 presents the estimated skewness A_φ of IMF azimuth distribution calculated from (5) separately for slow SW and trailing parts of high-speed streams. The estimated A_φ have relatively large statistical errors, especially in the period before 1995 when IMF measurements were comparatively rare. Nevertheless, we can note a fairly pronounced variation of A_φ in the 11-year cycle. Maxima of this variation occur during low solar activity, with small deviations in either direction from solar minimum. The amplitude of the skewness variation (change of A_φ from solar maximum to minimum) is, on average, ~ 0.2 in both slow and fast SW. Presumably, the amplitude slightly varies from cycle to cycle, but these variations can in part be due to statistical errors of estimates. We can observe that the A_φ values averaged over the long interval in slow and fast SW differ systematically. In slow SW (Figure 4, *a*), A_φ is on average close to zero, therefore the 11-year variation leads to a regular change of its sign. In the trailing parts of high-speed SW streams (Figure 4, *b*), on average $A_\varphi > 0$, and, as a rule, does not change its sign throughout the solar cycle (except for a short period near the solar maximum 1970–1971).

Quantitative studies of the azimuth distribution asymmetry and its variation with solar cycle have not probably been carried out before, although some changes

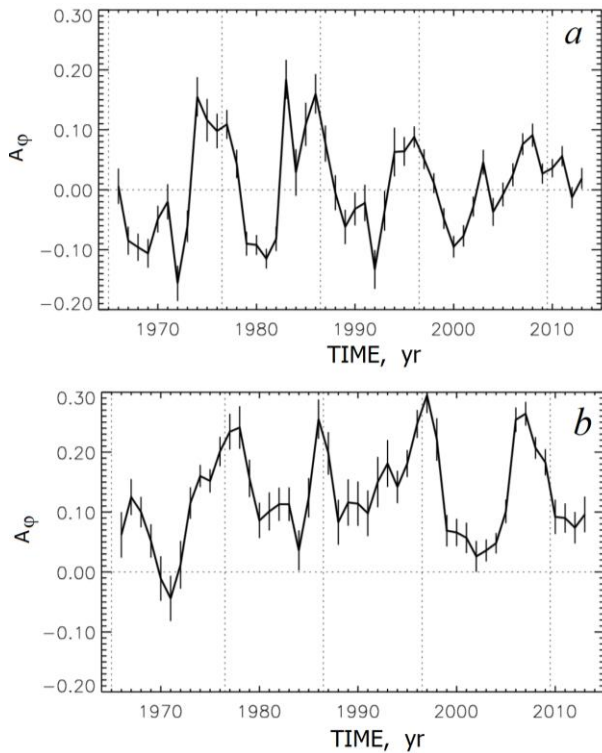


Figure 4. Skewness of IMF azimuth distribution A_φ as a function of time: slow SW (*a*); trailing parts of high-speed streams (*b*). Vertical dashes indicate probable errors of estimates. Solar minima are marked with vertical dotted lines

in the shape of the distribution with solar activity have been observed (see, e.g., [Borovsky, 2010]). As derived from the data presented in [Borovsky, 2010], the IMF azimuth distribution asymmetry can occur due to the presence of strong SW and magnetic field disturbances. Results of our calculation are, however, not directly affected by the strong disturbances, since the latter were excluded during data selection (see Section 1.1).

Figure 5 shows estimated A_θ of IMF elevation distribution calculated separately for slow SW and trailing parts of high-speed streams. Unlike the azimuth distribution asymmetry, the IMF elevation distribution asymmetry varies with the period of the magnetic (22-year) solar cycle, with A_θ being maximum in absolute magnitude during solar minima. This fact has been established in [Erofeev, 2014], in which θ distributions are plotted for solar minima at different orientations of the solar polar magnetic field. Let us note an interesting fact that although the sign of A_θ depends on the orientation of the solar polar magnetic field, it does not depend on IMF sector polarity (Figure 5 shows the result of the calculation from the sample including measurements in both the sectors). The amplitude of the 22-year A_θ variation varies from cycle to cycle; its value is, on average, ~ 0.25 in both slow and fast SW.

Figure 6 presents the time dependence of the correlation coefficient $C_{\varphi\theta}$ of φ and θ variations, calculated from Formula (6). The $C_{\varphi\theta}$ behavior is similar to the elevation asymmetry behavior described above: $C_{\varphi\theta}$ changes its sign with the period of the solar magnetic cycle, but it does not depend on the IMF sector polarity (this fact has been noted in [Erofeev, 2014]).

Thus, all the IMF angular characteristics considered

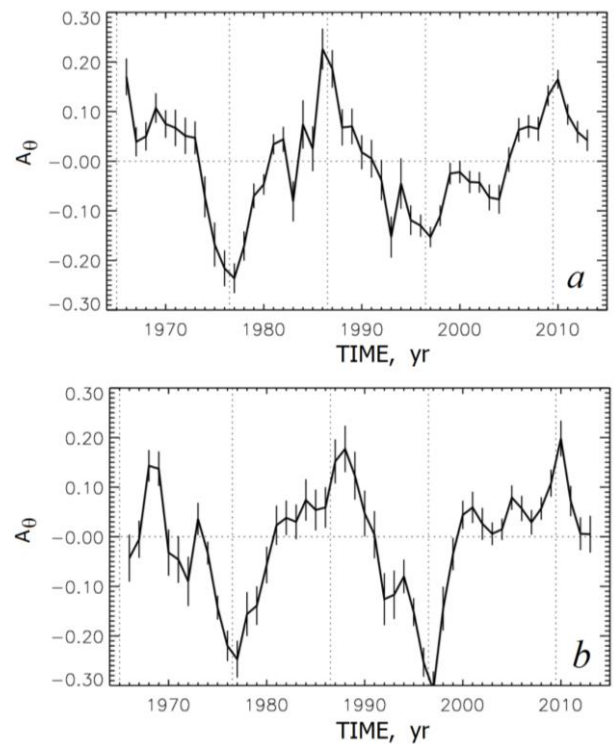


Figure 5. Skewness of IMF elevation distribution A_θ as a function of time: slow SW (*a*); trailing parts of high-speed streams (*b*). Vertical dashes indicate probable errors of estimates. Vertical dotted lines mark solar minima

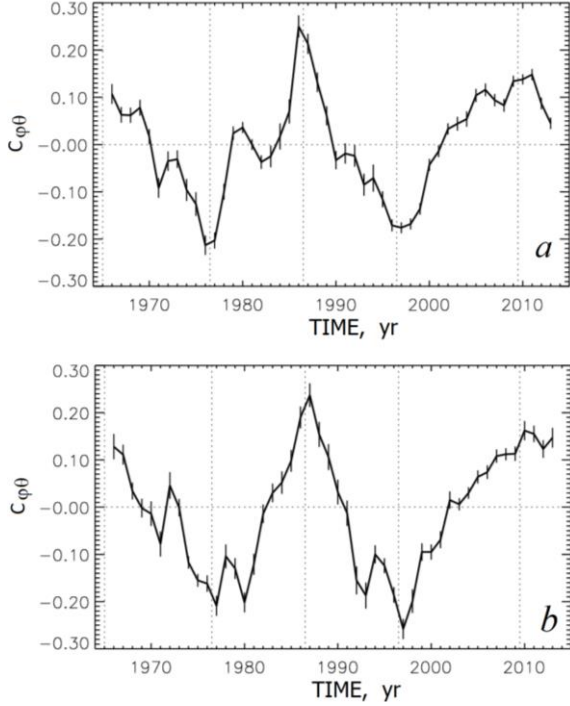


Figure 6. Correlation coefficient of IMF azimuth and elevation fluctuations as a function of time: slow SW (a); trailing parts of high-speed streams (b). Vertical dotted lines mark solar minima

regularly vary during solar cycle, two of them (the elevation distribution asymmetry and the φ and θ correlation) change sign depending on the direction of the solar polar magnetic field.

3. DESCRIPTION OF THE MODEL

The model considered is a generalization of the kinematic model proposed by Giacalone [2001]. The generalization involves taking into account SW stream inhomogeneities. Let (r, f, l) be the heliocentric distance, latitude, and longitude in the inertial reference system (see Figure 1, a), r_0 be the radius of the source surface, $\mathbf{V}(r, f, l, t)$ be the SW plasma velocity that when $r > r_0$ is radial, $\mathbf{V} = (V, 0, 0)$. The equations describing the evolution of magnetic field in the region $r > r_0$ have been derived from induction $\partial \mathbf{B} / \partial t = \text{rot}(\mathbf{V} \times \mathbf{B})$ and Maxwell $\text{div} \mathbf{B} = 0$ equations and have the following form:

$$\frac{d}{dt}(r^2 B_r) - \frac{r}{\cos f} \left(B_f \cos f \frac{\partial V}{\partial f} + B_l \frac{\partial V}{\partial l} \right) = 0, \quad (7a)$$

$$\frac{d}{dt}(r B_f) + r B_f \frac{\partial V}{\partial r} = 0, \quad (7b)$$

$$\frac{d}{dt}(r B_l) + r B_l \frac{\partial V}{\partial r} = 0, \quad (7c)$$

$$\frac{d}{dt} = \frac{\partial}{\partial t} + V \frac{\partial}{\partial r}. \quad (7d)$$

For $r > r_0$, the plasma element velocity is assumed to be constant, so $dV/dt = 0$ and $V(r, f, l, t) = V(r_0, f, l, t_0)$, where $t_0 = t - (r - r_0)/V$ (similar relations hold for the velocity gradients $\partial V / \partial f$ and $\partial V / \partial l$). The radial gradient of

SW velocity field arises when $\partial V / \partial l \neq 0$ due to the solar rotation with an angular velocity of Ω :

$$\frac{\partial V}{\partial r} = \frac{\Omega}{V} \frac{\partial V}{\partial l}.$$

The radial magnetic field component $B_r(r_0, f, l, t)$ and velocities $v_f(r_0, f, l, t)$ and $v_l(r_0, f, l, t)$ of random motions of magnetic footpoints are specified on the source surface. It is convenient to express the linear velocities v_f and v_l in terms of angular velocities w_f and w_l : $v_f = w_f r_0$, $v_l = w_l r_0 \cos f$. Due to the solar rotation and random motions of magnetic footpoints, transverse magnetic field components B_f and B_l are generated on the source surface:

$$B_f(r_0, f, l, t) = -B_r(r_0, f, l, t) \frac{r_0}{V} w_f(r_0, f, l, t), \quad (8a)$$

$$B_l(r_0, f, l, t) = -B_r(r_0, f, l, t) \frac{r_0 \cos f}{V} [w_l(r_0, f, l, t) + \Omega], \quad (8b)$$

which are then transported by the SW stream. Thus, IMF lines become distorted. Since the SW stream is nonuniform, random variations of the radial magnetic field component B_r are also generated during the transport of B_f and B_l random variations.

System of equations (7) with boundary conditions (8) can be solved by integrating over time in the reference system moving with the SW plasma element. The solution has the following form:

$$B_r(r_0, f, l, t) = B_r(r_0, f, l, t_0) P(r) \times \left\{ 1 - Q(r) \left[w_f(r_0, f, l, t_0) \frac{\partial V}{\partial f} + w_l(r_0, f, l, t_0) \frac{\partial V}{\partial l} \right] \right\}, \quad (9a)$$

$$B_f(r_0, f, l, t) = -B_r(r_0, f, l, t_0) P(r) \frac{r}{V} w_f(r_0, f, l, t_0), \quad (9b)$$

$$B_l(r_0, f, l, t) = -B_r(r_0, f, l, t_0) P(r) \frac{r \cos f}{V} [w_l(r_0, f, l, t_0) + \Omega], \quad (9c)$$

$$P(r) = \left(\frac{r_0}{r} \right)^2 \exp \left(- \frac{\partial V}{\partial l} \frac{\Omega (r - r_0)}{V^2} \right), \quad (9d)$$

$$Q(r) = \left[\exp \left(\frac{\partial V}{\partial l} \frac{\Omega (r - r_0)}{V^2} \right) - 1 \right] \left(\Omega \frac{\partial V}{\partial l} \right)^{-1}, \quad (9e)$$

where $t - t_0 = (r - r_0)/V$. In the simulation, we used a linear approximation for exponent (9e), which yields a simple approximation $Q = (r - r_0)/V^2$ with a relative error of $\sim 10\%$ at $r = 1$ AU and characteristic values $\partial V / \partial l$ (an exception is the interaction regions of fast and slow SW streams which we omit). The vector components \mathbf{B} in RTN are: $B_R = B_r$, $B_T = B_l$, $B_N = B_f$. Note that in studies of IMF direction the absolute value of $B_r(r_0, f, l, t_0) P(r)$, common to all the magnetic field components, is irrelevant. The value and specific form of the $|B_r|$ distribution over the source surface are therefore of little importance. However, we should take into account the sign

of $B_r(r_0, f, l, t_0)$ which determines the magnetic sector polarity.

Our model describes the evolution of IMF direction under the action of three factors: radial expansion of SW, twisting of the magnetic field into the Parker spiral, and impact of SW velocity gradients. The model is kinematic and therefore applicable to the study of large-scale relic variations of IMF lines, which have no time to undergo decay and development of turbulence when moving from the Sun to an observation point. For the measurements obtained in the near-Earth heliosphere, relic variations are variations with periods of several hours and more [Bruno, Carbone, 2005], hence their linear scales exceed 2×10^6 km.

If we know the parameters characterizing the SW velocity, the above model allows us to calculate the IMF angular distribution at given heliocentric distance and latitude (it is assumed that the distribution is averaged over the heliographic longitude and for a particular time interval, as is typically done in the experimental data analysis). To determine the IMF angular distribution requires taking a set of random values of angular velocities of motion of magnetic footpoints on the source surface w_l and w_f and using Formulas (9) and (1) to calculate a corresponding set of values of IMF azimuth and elevation φ and θ . In this paper, we use this approach to simulate variations of IMF angular distribution characteristics in the near-Earth region of the heliosphere during solar cycle ($r=1$ AU, $f \approx 0$). To do this, we calculate model samples of φ and θ under conditions characteristic of different phases of magnetic solar cycle. One sample corresponds to a time interval one year long and contains 10^4 estimates of φ and θ . The model samples of angle values are processed by the same method which is used in Section 2 for processing IMF measurements. As a result, we obtain time dependences of the IMF angular distribution characteristics similar to those derived from experimental data. The simulation is carried out separately for slow and fast SW (except for the interaction regions of fast and slow streams). Below we describe methods for setting parameters of the model.

In the model calculations, we assume that random motions of magnetic footpoints on the source surface have no preferred orientation, therefore the angular velocities w_l and w_f are independent random variables, and their standard deviations δw_l and δw_f are related by $\delta w_f = \delta w_l \cos f$. Thus, fluctuations of magnetic footpoints are characterized by one parameter $\delta w = \delta w_f$, which is considered to be independent of heliographic coordinates and time. The w_l and w_f velocities are assumed to be normally distributed random variables, and the δw value is chosen from the condition of the best agreement between model calculations and experimental data. Note that with this method of setting w_l and w_f the calculated samples of φ and θ characterize statistical properties of the ensemble of IMF lines observed in a random sequence. To simulate the time ordered series of measurements obtained by spacecraft instruments, we should take into account temporal and spatial correlations inherent in fluctuations of magnetic footpoints, but we have another purpose in this paper.

The SW velocity varies widely even if slow and fast SW are considered separately (see Figure 2, *a*). To take this fact into account, the SW velocity V in the simulation is set as follows. From the distributions shown in Figure 2, *a* relative frequencies P_i are determined at which velocity values fall into discrete cells of size 20 km/s with centers V_i , where i is the cell number. In the calculations, the SW velocity is assumed to be a discrete random variable taking values V_i with probabilities P_i . We suppose that there is no statistical relationship between the velocity values and other parameters of the model.

It is well known that except for the relatively narrow interaction regions of fast and slow SW streams we ignore, the SW velocity measured by spacecraft decreases with time due to the solar rotation. This indicates the presence of a large-scale longitudinal gradient of SW velocity. From OMNI-2 data we can estimate the mean longitudinal velocity gradient $G_l = \langle \partial V / \partial l \rangle$, which is equal to 1.3 km/s /deg. in slow SW and 3.7 km/s /deg. in trailing parts of high-speed SW streams. In the simulation, the large-scale longitudinal SW velocity gradient is assumed to be constant and equal to one of the above values of G_l .

Indirect data [Kojima et al., 1998] as well as direct measurements made by Ulysses instruments [Goldstein et al., 1996; McComas et al., 2000] have shown that during solar minima in the low-latitude region of the heliosphere there is a stable latitudinal SW velocity gradient negative in the southern hemisphere and positive in the northern one. The $|\partial V / \partial f|$ value can be as high as 10 km/s /deg. or higher at latitudes $\pm(10^\circ - 20^\circ)$. Details of the behavior of $\partial V / \partial f$ in the ecliptic plane are, however, poorly known because direct measurements of the latitudinal velocity gradient according to data from several spacecraft are sporadic (see [Crooker et al., 1997; Veselovsky, Shugay, 2010]). The presence of the latitudinal velocity gradient in the ecliptic plane is indirectly indicated by the presence of semi-annual and annual variations in the SW velocity measured in Earth's orbit during solar minima ([Zieger, Mursula, 1998]; see also the revised version of this article in *Geophys. Res. Lett.* 1998. V. 25, N 6. P. 2653). The available data, in particular the results obtained in [Crooker et al., 1997], allows us to suppose that during solar minima the surface separating heliospheric regions with different signs $\partial V / \partial f$ coincides roughly with the heliospheric current sheet (HCS). Thus, $\partial V / \partial f > 0$ and $\partial V / \partial f < 0$ are respectively north and south of HCS. Since HCS is inclined to the equatorial plane [Smith, 2008], in the equatorial zone of the heliosphere the sign of $\partial V / \partial f$ depends on heliographic longitude and, on average, $\partial V / \partial f \approx 0$. However, since HCS also separates regions with different IMF polarities (magnetic sectors), within each of the sectors $\partial V / \partial f$ has a constant sign and, on average, is not zero. Depending on the orientation of the solar polar magnetic field, the IMF radial component B_R and the latitudinal velocity gradient have either the same sign or opposite signs. In view of these facts, the variation in the latitudinal SW velocity gradient during the 22-year cycle in the model calculations is given by the expression

$$\frac{\partial V}{\partial f} = -\text{sign}(B_R) G_f \cos^3 \left[\frac{2\pi(t-t_m)}{T} \right], \quad (10)$$

where $\text{sign}(B_R)$ is the IMF sector polarity, G_f is the amplitude of the variation, T is the period of the solar magnetic cycle, and the origin of the time t_m corresponds to the epoch of solar minimum when magnetic polarity at the south pole of the Sun was positive (such a situation occurred during solar minima in 1965, 1986, and 2009). The use of expression (10) means that in the simulation the change of sign of $\partial V/\partial f$ in the ecliptic plane is taken into account, but the dependence of the absolute value of $\partial V/\partial f$ on heliographic coordinates is ignored. The amplitude of the latitudinal velocity gradient variation G_f is taken to be constant and its value is chosen based on the best agreement between model calculations and experimental data.

The consideration of regular, i.e. constant or varying on the time scale of the 11-year cycle, SW velocity gradients too roughly describes the real situation because the SW stream comprises inhomogeneities with relatively small scales and short lifetimes. We will call such inhomogeneities and their associated velocity gradients local. Referring to the preliminary calculations [Erofeev, 2017], local SW inhomogeneities have a significant effect on the IMF angular distribution. In the simulation, their effect can be taken into account by adding random variations to regular SW velocity gradients. In practice, the random variations of latitudinal and longitudinal velocity gradients are set independent normally distributed random values with identical standard deviations δG . The parameter δG is regarded as time independent, and its value is varied to achieve the best quantitative agreement between the model and experimental estimates.

The calculations show that the choice of the radius of the source surface r_0 has almost no effect on the simulation results when the condition $r_0 \ll r$ holds. This conclusion can be drawn directly from (9) if we ignore the distance dependence of the magnetic field modulus. Thus, the presence of r_0 in our kinematic model is to a certain extent formal, and the value of this parameter can always be chosen large enough to satisfy the condition of predominance of SW kinetic energy over the magnetic field energy. In particular, we can choose r_0 dependent on heliographic latitude and/or SW velocity, then the source surface would have a non-spherical shape. The results presented below (see Section 4) have been obtained at a constant value of $r_0=0.015$ AU (three solar radii).

Thus, the model considered has three free parameters: amplitude of random velocities of motion of magnetic footpoints on the source surface δw , amplitude of variation of the latitudinal SW velocity gradient G_f in a solar cycle, and rms value of local velocity gradients δG . In this case, the latitudinal velocity gradient is the only characteristic of SW stream, which is assumed to be regularly varying in the course of solar cycle.

4. SIMULATION RESULTS AND COMPARISON WITH EXPERIMENTAL DATA

When comparing the simulation results with the results of the experimental data analysis, we have compared time dependences of five characteristics of the IMF angular distribution: RMSDs S_φ and S_θ , skewness A_φ and A_θ , and correlation $C_{\varphi\theta}$. The model was quantitatively fitted to the experimental data by comparing mean values of these characteristics, as well as mean values of amplitudes of their variations in a solar cycle (the behavior of the correlation coefficient $C_{\varphi\theta}$ was compared only in qualitative terms). The best agreement with the experimental data was obtained for slow SW when values of free parameters of the model $\delta w=2.5 \cdot 10^{-6}$ rad/s, $G_f=5.4$ km/s/deg., $\delta G=4.2$ km/s/deg., and for fast SW when $\delta w=2.7 \cdot 10^{-6}$ rad/s, $G_f=6.5$ km/s/deg., $\delta G=5.3$ km/s/deg. Since this quantitative agreement is not ideal, the given values of the model parameters (hereinafter called optimal values) are only approximately estimated SW characteristics. The calculation results at the optimal values of the model parameters are shown in Figures 7 (for slow SW) and 8 (for fast SW). The time dependence of the IMF angular distribution characteristics shown in these Figures has random fluctuations due to the limited size of the model samples of φ and θ .

Consider the simulated time dependences of RMSD of φ and θ (Figures 7, *a* and 8, *a*). With optimal values of model parameters the mean values of S_φ and S_θ are consistent with the experimental estimates up to $\sim 10\%$. In particular, the model calculation simulates the excess of S_φ over S_θ by $\sim 10^\circ$. As noted in Borovsky [2010], the inequality $S_\varphi > S_\theta$ can be caused by the geometric effect associated with an asymmetric method of determining the φ and θ angles of the spherical coordinate system. The said geometric effect undoubtedly affects estimates of RMSD of φ and θ , but the calculations have shown S_φ changes significantly under the action of kinematic effects, whereas S_θ changes insignificantly. The systematic difference between S_φ and S_θ is therefore determined mainly by the presence of SW velocity gradients. At high solar activity, S_φ is affected by the constant longitudinal velocity gradient and local SW inhomogeneities, and at solar minima it is also affected by the large-scale latitudinal velocity gradient. Consequently, S_φ varies in the 11-year cycle, reaching maximum values during solar minima. The presence of the 11-year variation in S_φ is consistent with the experimental data analysis results. The analysis of IMF measurement (Section 2) has also shown a small increase in S_φ and S_θ at high solar activity. In general, the model does not simulate this variation in angular RMSD, although in the case of slow SW the simulated time dependence of S_θ exhibits weak regular variations that occur in phase with solar activity variations (see Figure 7, *a*). The increase in RMSD of φ and θ during maxima of the 11-year cycle is likely to be caused not by kinematic effects but by a small (5–10 %) increase in the amplitude of fluctuations of IMF footpoints.

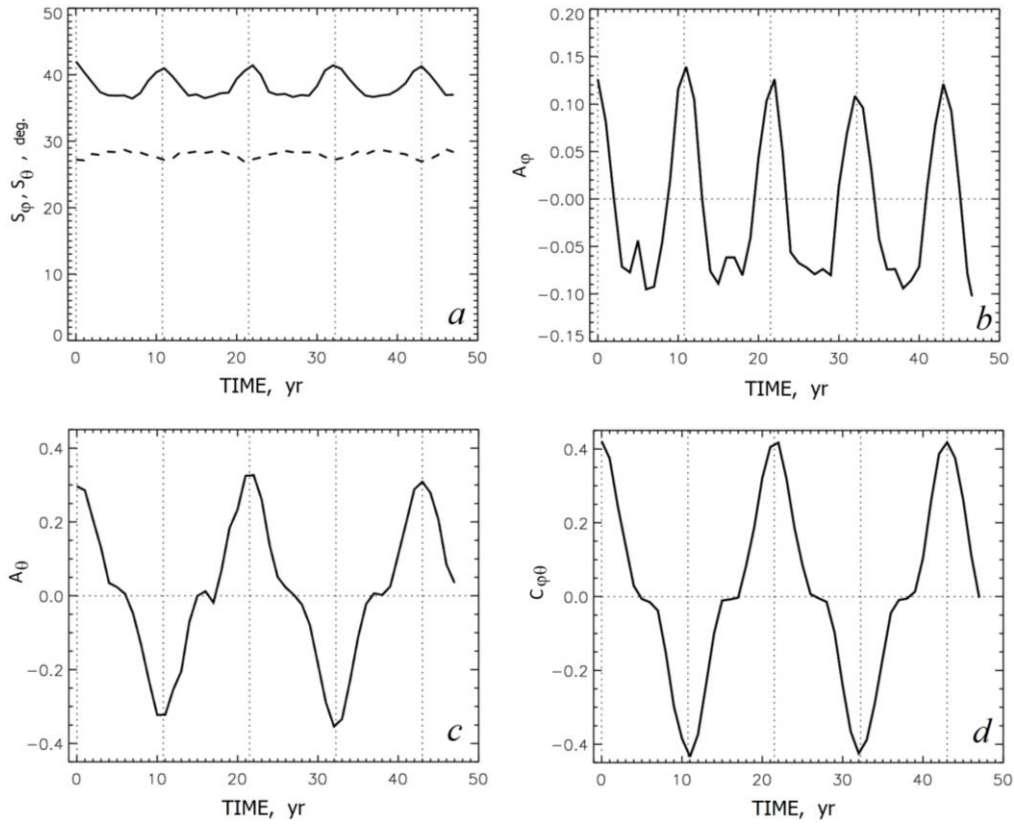


Figure 7. Simulated time dependences of IMF angular distribution characteristics for slow SW: RMSDs of IMF azimuths and elevations (*a*, solid and dashed lines); skewness of IMF azimuth distribution (*b*); skewness of IMF elevation distribution (*c*); correlation coefficient (*d*)

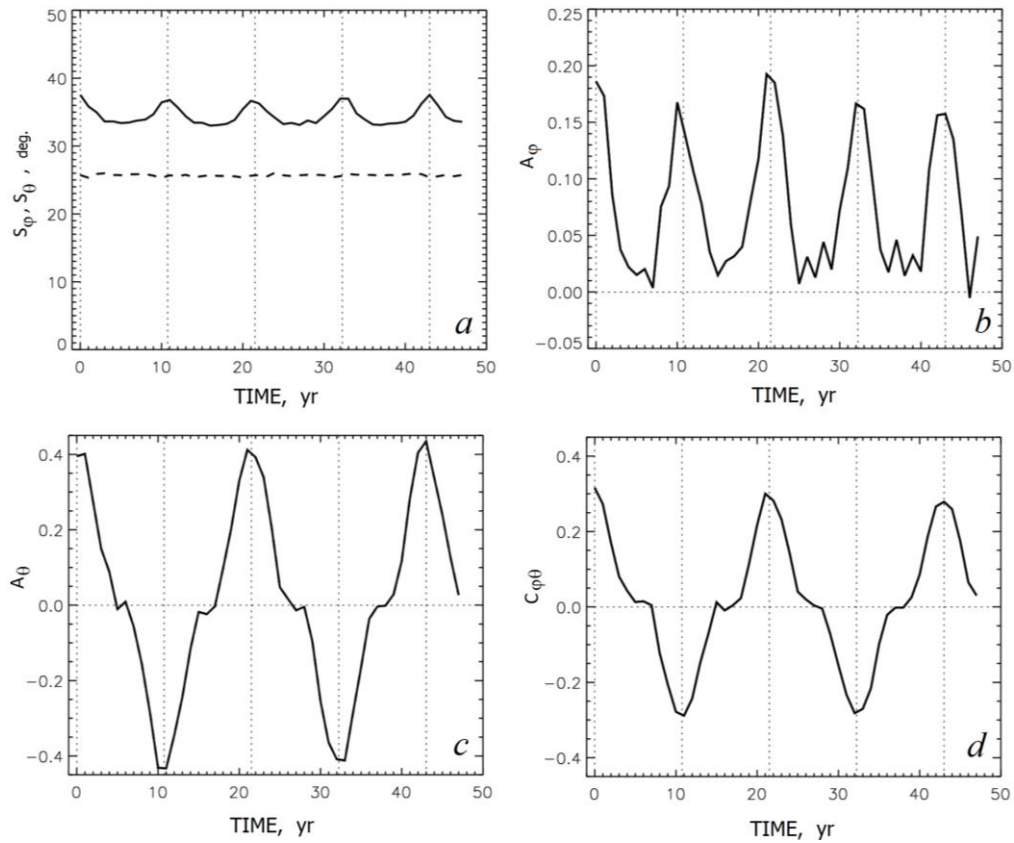


Figure 8. The same as in Figure 7 for trailing parts of high-speed SW streams

The simulated time dependences of the skewness of the IMF azimuth distribution (Figure 7, *b* and 8, *b*) demonstrate the 11-year variation in A_φ with maxima during solar minima. Such a variation in A_φ has been obtained from the experimental data analysis (see Section 2). At optimal values of the model parameters, amplitudes of the 11-year A_φ variation in slow and fast SW are approximately equal and close to the value of 0.2 derived from the experimental data. Besides, the average value of A_φ is zero in slow SW (see Figure 7, *b*) and significantly positive in fast SW (see Figure 8, *b*), which also agrees with results of the experimental data analysis. In general, the quantitative agreement between the model and experimental data for A_φ is $\sim 30\%$. Here are some details that explain the influence of different components of SW inhomogeneities on the behavior of A_φ . In the absence of SW velocity gradients, the φ distribution is strongly asymmetric with $A_\varphi < 0$. The cause is the twisting of IMF into the Parker spiral, which violates the symmetry of magnetic field fluctuations relative to the direction of unperturbed field lines (for more detail see [Erofeev, 2017]). The effect of the SW velocity gradients, however, reduces the negative asymmetry of the φ distribution in modulus, and at sufficiently large velocity gradients A_φ changes its sign to positive (examples of the φ angle distributions for different characteristics of SW inhomogeneity are given in [Erofeev, 2017]). At high solar activity, the change of A_φ toward positive values is due to the influence of local SW inhomogeneities as well as longitudinal velocity gradient. The presence of a significant longitudinal velocity gradient in trailing parts of high-speed SW streams partly explains the difference between the average values of A_φ in slow and fast SW. During solar minima, the azimuth distribution asymmetry is further affected by the large-scale latitudinal velocity gradient, which leads to the 11-year A_φ variation.

The simulated time series of elevation skewness A_θ (Figure 7, *c* and 8, *c*) and angular correlation coefficient $C_{\varphi\theta}$ (Figure 7, *d* and 8, *d*) show variations with the period of the 22-year magnetic cycle, which occur in phase in positive and negative IMF sectors (Figures 7, 8 present results for the positive sector). Such behavior of A_θ and $C_{\varphi\theta}$ is due to the following facts. As shown by the model calculations, A_θ and $C_{\varphi\theta}$ are odd functions of $\partial V/\partial f$, therefore they differ from zero only in the presence of the large-scale latitudinal SW velocity gradient, which occurs during low solar activity. Moreover, signs of A_θ and $C_{\varphi\theta}$ depend on the sign of the radial magnetic field component on the source surface B_R , i.e. on IMF sector polarity. As a result, A_θ and $C_{\varphi\theta}$ coincide in sign with the expression $-B_R \partial V/\partial f$. The sign of this expression depends on the orientation of the solar magnetic fields, and not on the IMF sector polarity (see discussion in Section 3). Thus, the model qualitatively explains the features of the behavior of A_θ and $C_{\varphi\theta}$ found in the experimental data analysis (see Section 2). Quantitatively, the agreement with the experimental data for A_θ is somewhat worse than that for other characteristics of the IMF angular distribution. At optimal values of the model

parameters, the mean value of the amplitude of the 22-year A_θ variation appears to be overestimated compared to the experimental data processing results approximately by a factor of 1.4 for slow SW and 1.7 for fast SW. This discrepancy cannot be corrected by changing the free parameters of the model without significant deterioration in the quantitative agreement with the experimental data in other characteristics of the IMF angular distribution. The amplitude of the 22-year variation of the correlation coefficient $C_{\varphi\theta}$ is also overestimated as compared to the IMF measurement processing results. These discrepancies can formally be explained by the presence of uncorrelated fluctuations of φ and θ in the experimental data, which are not described by our model. A physical cause of such variations may be the partial turbulent decay of relic magnetic field fluctuations, which occurs when they are transferred from near-Sun space to the heliocentric distance of 1 AU.

5. CONCLUSIONS AND DISCUSSION

To calculate quantitative parameters of the IMF angular distribution, we have used 48-year series of hourly average magnetic field vector measurements obtained in near-Earth orbits. The measurements made during strong SW disturbances (in particular, in interaction regions of fast and slow SW streams) were excluded from the original series. We have obtained the following results.

The root mean square deviations (RMSD) of IMF azimuth and elevation vary during the solar cycle. These variations have two components: The first is an $\sim 15\%$ increase in RMSD of azimuth during solar minima; the second, a weaker component, leads to a small increase in RMSD of IMF azimuth and elevation during solar maxima. RMSDs of azimuths are systematically higher than those of IMF elevations.

The skewness A_φ of the IMF azimuth distribution exhibits a variation in the course of solar cycle, being maximum during minima of 11-year cycles. There is a systematic difference in A_φ between slow SW and trailing parts of high-speed streams.

The skewness A_θ of IMF elevation distribution varies during the solar cycle, the absolute values of A_θ being maxima during minima of 11-year cycles. The sign of A_θ depends on the orientation of the solar polar magnetic field but does not depend on the IMF sector polarity.

The correlation coefficient $C_{\varphi\theta}$ of IMF azimuth and elevation fluctuations varies during the solar cycle, reaching extrema during minima of 11-year cycles. The sign of $C_{\varphi\theta}$ depends on the orientation of the solar polar magnetic field but does not depend on the IMF sector polarity.

Some of the above experimental data analysis results have been obtained earlier in [Burlaga, Ness, 1997; Borovsky, 2010; Erofeev, 2014], which used slightly different methods of IMF measurement processing. The new conclusions are probably those about the behavior of the skewness of IMF azimuth distribution, as well as the established relationship of variations in RMSD of IMF azimuths with phase of the 11-year solar cycle.

The comparison between the results of simulation of

the IMF angular distribution and the results of the experimental data analysis has shown that in a qualitative sense their agreement can be regarded as satisfactory. The model mainly simulates variations of five basic parameters of the IMF angular distribution in a solar cycle: RMSD of angles (IMF azimuth and elevation), asymmetries of the distributions of the angles, and correlation coefficient of azimuth and elevation. These variations are caused by a regular variation of the latitudinal velocity gradient in the equatorial region of the heliosphere. Note that the latitudinal SW velocity gradient causes not only a change in the shape of IMF azimuth and elevation distributions but also the appearance of angle correlation, i.e. anisotropy of magnetic field fluctuations. Some features of the behavior of the IMF angular distribution can also be explained by the presence of the constant longitudinal SW velocity gradient and local SW inhomogeneities. The only regular variation that is found in the analysis of measurements and is not simulated by the model is a slight increase in RMSD of IMF azimuth and elevation during solar maxima. This variation is probably caused by a change in the amplitude of the random motions of magnetic footpoints, i.e. is not a direct consequence of the SW stream inhomogeneity.

The quantitative agreement between the model and experimental data in general can also be recognized as satisfactory, taking into account that the model has a minimum number of free parameters. Important characteristics of the model (such as latitude-longitude dependence of the velocity gradient in the ecliptic plane and statistical properties of magnetic footpoint fluctuations) are poorly known and specified based on the simplest assumptions. It is likely that the parameters, which were considered constant in the simulation, in fact slightly vary during the solar cycle as well as on a large time scale. Furthermore, these parameters may depend on heliographic latitude and longitude. Such space and time dependences of parameters can be included in the model to improve the quantitative agreement with experimental data. The consideration of the additional effects with the poorly known characteristics, however, requires increasing the number of free parameters of the model, which in the end does not enhance confidence in the simulation results. On the other hand, the approximate agreement with the experimental data obtained for the simplest version of the model suggests that various additional effects do not play a fundamental role in the formation of the IMF angular distribution at heliocentric distances up to 1 AU.

The model considered has a limited applicability because it describes the evolution only of large-scale relic perturbations of IMF lines in a limited range of heliocentric distances. The model, however, demonstrates an essential role of kinematic effects associated with the presence of SW velocity gradients and may be useful for some applications. In addition to the calculation of the IMF angular distribution, the model can be used to examine the geometry of large-scale perturbations of magnetic field lines. The field line geometry has an effect on the transport of charged particles in the helio-

sphere and probably on the impact of IMF disturbances on magnetospheres of Earth and other planets. Besides, large-scale variations in IMF direction can affect anisotropy and other parameters of the small-scale turbulence generated in SW.

The experimental data in use was obtained from the archive of the National Space Science Data Center and Space Physics Data Facility [http://nssdcftp/gsf.nasa.gov/spacecraft_data].

REFERENCES

- Borovsky J.E. On the variations of the solar wind magnetic field about the Parker spiral direction. *J. Geophys. Res.* 2010, vol. 115, A09101. DOI: [10.1029/2009JA015040](https://doi.org/10.1029/2009JA015040).
- Bruno R., Carbone V. The solar wind as a turbulence laboratory. *Living Rev. Solar Phys.* 2005, vol. 2, pp. 1–186. <https://link.springer.com/article/10.12942/lrsp-2005-4>.
- Burlaga L.F., Ness R.F. Global patterns of heliospheric magnetic field polarities and elevation angles: 1990 through 1995. *J. Geophys. Res.* 1997, vol. 102, no. A9, pp. 19,731–19,742. DOI: [10.1029/97JA01568](https://doi.org/10.1029/97JA01568).
- Crooker N.U., Lazarus A.J., Phillips J.L., Steinberg J.T., Szabo A., Lepping R.P., Smith E.J. Coronal streamer belt asymmetries and seasonal solar wind variations deduced from Wind and Ulysses data. *J. Geophys. Res.* 1997, vol. 102, no. A3, pp. 4673–4679. DOI: [10.1029/96JA03681](https://doi.org/10.1029/96JA03681).
- Erofeev D.V. Variation in the statistical properties of IMF direction fluctuations during the 22-year solar magnetic cycle. *Geomagnetism and Aeronomy.* 2014, vol. 54, no. 8, pp. 1032–1038. DOI: [10.1134/S0016793217070064](https://doi.org/10.1134/S0016793217070064).
- Erofeev D.V. Model of transport of large-scale magnetic field fluctuations in the solar wind. *Geomagnetism and Aeronomy.* 2017, vol. 57, no. 7, pp. 864–868. DOI: [10.1134/S0016793217070064](https://doi.org/10.1134/S0016793217070064).
- Forsyth R.J., Balogh A., Smith E.J., Erdos G., McComas D.J. The underlying Parker spiral structure in the Ulysses magnetic field observations, 1990–1994. *J. Geophys. Res.* 1996, vol. 101, no. A1, pp. 395–403.
- Giacalone J. The latitudinal transport of energetic particles associated with corotating interaction regions. *J. Geophys. Res.* 2001, vol. 106, no. A8, pp. 15,881–15,887.
- Giacalone J., Jokipii J.R. Magnetic footpoints diffusion at the Sun and its relation to the heliospheric magnetic field. *Astrophys. J.* 2004, vol. 616, pp. 573–577. DOI: [10.1086/424870](https://doi.org/10.1086/424870).
- Goldstein B.E., Neugebauer M., Phillips J.L., Bame S., Gosling J.T., McComas D., Wang Y.-M., Sheeley N.R., Suess S.T. Ulysses plasma parameters: latitudinal, radial, and temporal variations. *Astron. Astrophys.* 1996, vol. 316, pp. 296–303.
- Kojima M., Tokumaru M., Watanabe H., Yokobe A. Heliospheric tomography using interplanetary scintillation observations 2. Latitude and heliocentric distance dependence of solar wind structure at 0.1–1 AU. *J. Geophys. Res.* 1998, vol. 103, no. A2, pp. 1981–1989. DOI: [10.1029/97JA02162](https://doi.org/10.1029/97JA02162).
- Kovalenko V.A. *Solnechniy veter* [Solar Wind]. Moscow, Nauka Publ., 1983. 272 p. (In Russian).
- Lyatsky W., Tan A., Lyatskaya S. Effect of the Sun's magnetic field polarity on interplanetary magnetic field B_z . *Geophys. Res. Lett.* 2003, vol. 30, L2258. DOI: [10.1029/2003GL017431](https://doi.org/10.1029/2003GL017431).
- Mardia K.V. *Statistics of directional data*. London & New York, Academic Press. 1972, 380 p.
- McComas D.J., Barraclough B.L., Funsten H.O., Gosling J.T., Santiago-Munoz E., Skoug R.M., Goldstein B.E., Neugebauer M., Riley P., Balogh A. Solar wind observations over Ulysses' first full polar orbit. *J. Geophys. Res.* 2000, vol. 105, no. A5, pp. 10,419–10,433. DOI: [10.1029/1999JA000383](https://doi.org/10.1029/1999JA000383).

Schwadron N.A., McComas D.J. The sub-Parker spiral structure of the heliospheric magnetic field. *Geophys. Res. Lett.* 2005, vol. 32, L03112. DOI: [10.1029/2004GL021579](https://doi.org/10.1029/2004GL021579).

Smith E.J. The global heliospheric magnetic field. *The Heliosphere through the Solar Activity Cycle*. Springer, 2008, pp. 79–150.

Tu C.-Y., Marsch E. A Model of solar wind fluctuations with two components: Alfvén waves and convective structures. *J. Geophys. Res.* 1993, vol. 98, no. A2, pp. 1257–1276.

Ulrich K., Tran T. Generation of a North/South magnetic field component from variations in the photospheric magnetic field. *Solar Phys.* 2016, vol. 291, pp. 1059–1076. DOI: [10.1007/s11207-016-0882-5](https://doi.org/10.1007/s11207-016-0882-5).

Veselovsky I.S., Tarsina M.V. Angular distribution of interplanetary magnetic field vector. *Geomagnetizm i aeronomiya* [Geomagnetism and Aeronomy]. 2001, vol. 41, no. 4, pp. 471–476. (In Russian).

Veselovsky I.S., Shugay Yu.S. High-speed flows of solar wind near the Earth's orbit and their sources on the Sun from stereoscopic observations during minimum of cycle 23. *Kosmicheskiye issledovaniya* [Cosmic Res.]. 2010, vol. 48, no. 1, pp. 33–42. (In Russian).

Xu F., Li G., Zhao L., Zhang Y., Khabarova O., Miao B., le Roux J. Angular distribution of solar wind magnetic field vector at 1 AU. *Astrophys. J.* 2015, vol. 801, iss. 1, article id. 58, 7 p. DOI: [10.1088/0004-637X/801/1/58](https://doi.org/10.1088/0004-637X/801/1/58).

Zieger B., Mursula K. Annual variation in near-Earth solar wind speed: Evidence for persistent north-south asymmetry related to solar magnetic polarity. *Geophys. Res. Lett.* 1998, vol. 25, no. 6, pp. 841–844.

URL: ftp://nssdcftp/gsfc.nasa.gov/spacecraft_data (accessed October 1, 2018).

How to cite this article

Erofeev D.V. Effect of large-scale inhomogeneity of solar wind velocity on distribution of directions of interplanetary magnetic field vector. *Solar-Terrestrial Physics*. 2019. Vol. 5. Iss. 3. P. 42–53. DOI: [10.12737/stp-53201905](https://doi.org/10.12737/stp-53201905).